Thermo-mechanical deformation degradation of crystalline silicon photovoltaic (c-Si PV) module in operation

*Emeka H. Amalu, David J. Hughes, F. Nabhani and Julie Winter

Department of Engineering, School of Science, Engineering and Design, Teesside University, Middlesbrough, Teesside Valley, TS1 3BA, UK.

*E-mail address: E.Amalu@tees.ac.uk; Tel.: +44(0)1642342450

Abstract

Reliability and mean-time-to-failure (MTTF) of crystalline silicon photovoltaic (c-Si PV) module operating at elevated temperature can be increased through in-depth understanding of the mechanics of thermo-mechanical deformation and degradation of the laminates bonded together in the system. The knowledge is critical to developing the next generation of robust c-Si PV modules. Deployment in elevated ambient temperature reduces the 25-year design life by inducing excessive deformation that results in significant laminate degradation. The research investigates the thermo-mechanical deformation of c-Si PV module. Analytical and simulation methods are employed in the investigation. The IEC 61215 test qualification is used. Ethylene vinyl acetate (EVA) and solder materials responses are modelled as temperature dependent with appropriate material models. Analytical technique for validating simulation results of the response of c-Si PV module to temperature load is presented. The laminate's stiffness is found to be governed by the stiffness ratio magnitude of silicon which is the most stressed component. The deformation ratio of EVA is highest and significantly determines the degree of variation of gap between solar cells. The EVA exhibits the highest susceptibility to thermo-mechanical deformation followed by the solder which is found to accumulate the highest magnitude of strain energy density. The research presents an analytical method that can be used to validate the output of computer-simulation of the magnitude of strain energy density of solder in c-Si PV modules.

Keywords

Crystalline silicon photovoltaic (c-Si PV) module, Deformation mechanics, Solder strain energy density, Finite element modelling (FEM), Analytical models, Ambient temperature.

1. Introduction

The realisation that the sun generates in just an hour the total magnitude of electrical power consumed annually on the entire planet makes photovoltaic modules attractive as the ultimate renewable energy resource. The global adoption and use of the photovoltaic (PV) modules as the main source of energy is the key to realising the UN Millennium

Development Goals (UN MDG) on Green Energy. The universal acceptance of the PV technology, projected to contribute about 20% of world energy supply by 2050, over 60% by 2100 and leading to 50% reduction in global CO_2 emissions, is threatened by its poor performance in the tropical climates - which leads to its low deployment in the region. The crystalline silicon photovoltaic (c-Si PV) module is reported by Ogbomo et al 2017 [1] to demonstrate best power conversion efficiency (PCE) of 25 %, highest market share of 84% and energy payback time (EPBT) of about 48 months. The identification that silicon solar cells are the most viable option suitable for large volume production [2, 3] makes further research on the technology necessary – in repositioning for the global uptake.

The design and development of the next generation of robust and reliable crystalline silicon photovoltaic (c-Si PV) modules is hugely dependent on the in-depth knowledge and understanding of the mechanics of thermo-mechanical deformation and degradation of laminates in the module. The knowledge and understanding will inform on the design considerations of the critical parameters and requirement of the next generation of the module. The requirements include ensuring that the gap between solar cells is minimum and sufficient to accommodate the module thermal expansion at elevated temperature operations. Inaccurate design of the solar cell gap leads to micro-crack initiation on stressed cells. Cracked cells negatively impact on cell performance and module efficiency. Excessive cell gap leads to loss of useful cell space which impact on cell density and module's power output.

In a recent research, Zarmai et al 2015 [3], reviewed interconnection technologies for improved c-Si PV module assembly and reported that McCluskey [4] and Campeau, et al [5] had reported that per a BP study, 40.7% of PV module failures observed were due to cell or interconnect breakage. The most susceptible component of c-Si PV module interconnection to degradation and failure is the solder joints. In a similar study, Ogbomo et al 2017 [1] reported that numerous studies which include [6] had reported similar findings. They also reported that the failure figure is higher in the tropical climate.

Thermo-mechanical degradation of solder interconnections in c-Si PV module assembly is caused by the coefficient of thermal expansion (CTE) mismatch between bonded laminate materials. During operations of c-Si PV module in elevated ambient temperatures, module temperature rises from the standard test condition (STC) up to 85°C at the peak of the day and subsequently falls as the day progresses. The temperature cycling repeats every day and night. The repeated cycling induces thermo-fatigue issues that culminate in failure after long operations. Failure usually starts from solder joint cracking to crack propagation and eventually failure of the module.

Fig 1.1 shows a typical c-Si PV module. The Fig 1.1 (a) is a module that has 72 cells interconnected together. The gaps between the solar cells can be seen. The Fig 1.1 (b) shows a finite element (FE) model of two silicon solar cells interconnected together while the Fig 1.1 (c) shows the portion of the c-Si PV module laminate being investigated. The module is a multilayer assembly of different materials possessing different properties. The component materials include: glass superstrate, solar cells interconnected together with copper ribbons, encapsulating polymer - ethylene vinyl acetate - (EVA), polymeric

protective backsheet called tedlar polyester tedlar (TPT), solder used to attach the copper ribbons to silver metallization on top of silicon cells and thin aluminium metallization on the back of the solar cells. A schematic full structure of the portion of the module laminates being investigated is shown in Fig 3.1. Paggi et al 2011 [7] stated that a typical distance between the neighbouring solar cells is 2 mm and the solar span is 125 mm or 156 mm.

Realising robust and reliable c-Si PV modules is critical to meeting the UN Millennium Development Goals on Green Energy. The robust c-Si PV module will perform consistently up to the 25-year design lifespan even while operating in elevated ambient temperatures. The benefits of actualising the robust and reliable module include wide global adoption of the technology and increased deployment in the tropical climate - where its reliability and performance are currently an issue.

This research studies the deformation of materials and the degradation of solder joints in c-Si PV module laminates to provide knowledge and understanding of the mechanics concepts which can be employed to design and develop the next generation of c-Si PV module with improved reliability at elevated temperature operations.

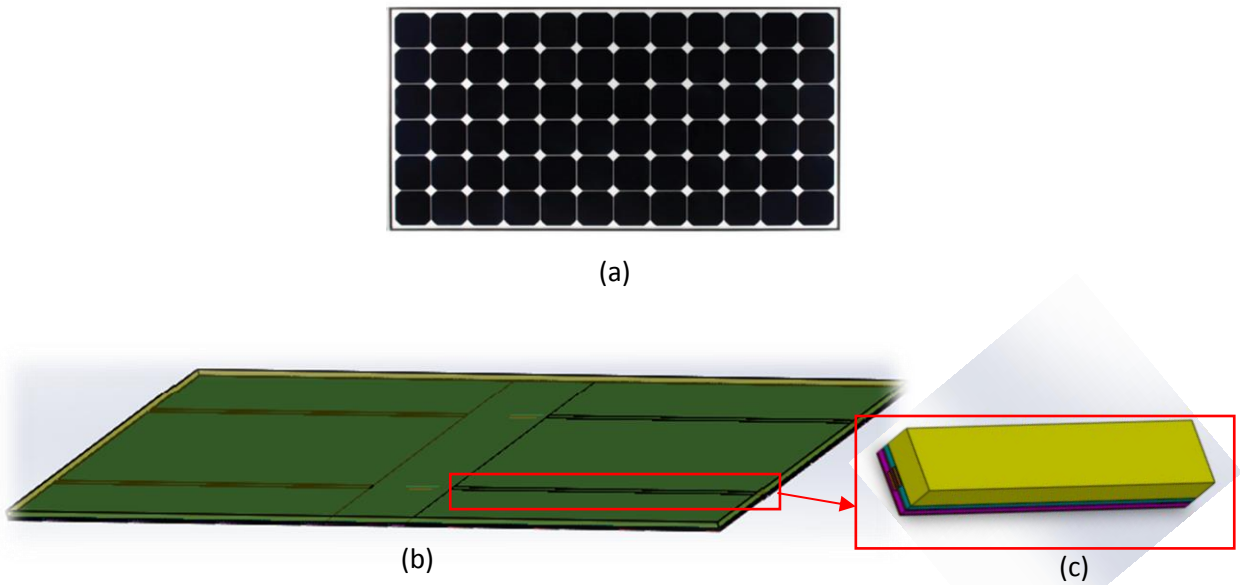

Fig.1.1: A typical crystalline silicon PV module showing:
(a) A module with 72 cells interconnected together and display gaps between solar cells.
(b) A finite element model of two solar cells interconnected together.
(c) An area of the FE model being investigated.

2. State of investigation

A review of relevant literature is conducted on the state-of-the-art and the challenges of designing and producing the next generation of c-Si PV module that will possess improved thermo-mechanical reliability at elevated temperature operations. Current

research on fatigue life, reliability, thermo-mechanical response and influence of elevated temperature on structures, composites and laminates includes Lyubimova, L.L et al 2017[8], Mejri et al 2017[9] and Khashaba et al 2017 [10]. A better understanding of the thermo-mechanical deformation degradation of the laminates is found to be the key to designing the required module. The understanding depends on an in-depth knowledge of the properties of materials in the laminates in addition to developing a mechanism to validate the result of computer simulation of the module response to externally applied loads. This section presents and discusses the state of the investigation in two sub-sections. These are the material model and the analytical method.

2.1 Material model

The use of appropriate material model is key to determining the accurate magnitude of critical c-Si PV module design factors. These factors include the gap between solar cells, thermo-mechanical stresses, strains and strain energy density of the solder and other components in the c-Si PV module laminates. The vital materials whose model is considered in this research include EVA and tin-lead (SnPb) solder.

2.1.1: EVA material: It is found that EVA is modelled as linear elastic material in some investigations. This assumption leads to an inaccurate estimation of the design parameters. Current research which include [7, 11-13] have demonstrated the need to model EVA as visco-elastic material in addition to modelling the Young's modulus of elasticity, E, as temperature dependent. Variations on the models employed in previous research exist and there is need to unify the models – for universal adoption. In this research, a suitable material model for EVA is adopted by utilising the plot in Fig 2.1 from Paggi et al 2011 [7].

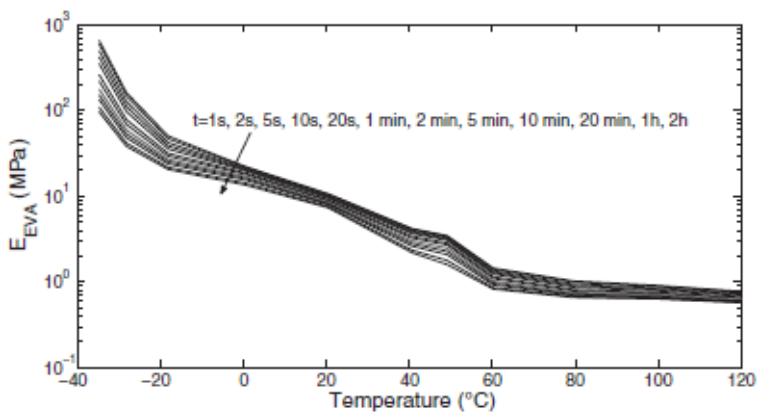

Fig 2.1: Elastic modus of EVA versus temperature for different relaxation times.

2.1.2: Solder material: It is found that some research have not modelled the Young's modulus of tin-lead (SnPb) solder as temperature dependent. The practice is likely to introduce inaccuracy in the simulation result. The response of SnPb solder to the

cyclic ambient temperature is modelled with either creep relations or visco-plastic models. In this investigation, both the creep and visco-plastic models are employed to model the solder response. The approach allows for comparison of the results generated from their use. Further details on material models employed in this research is provided in material and their properties sub-section of the finite element modelling (FEM) section.

2.2 Analytical method to validate computer simulation output for solder strain energy/energy density as well as magnitude of deformation for c-Si PV module laminate.

There is a need to develop both technique and analytical models to validate the computer simulation output of the magnitude of solder strain energy/energy density from FEM. It is found that the magnitude of SnPb solder strain energy density reported by numerous investigations which include [12, 14-18] on c-Si PV module and other electronic modules is in the magnitude of kPa to MPa. Thus, it becomes imperative to develop technique and an analytical model to validate the results of the computer simulation output. Similarly, it is also important to develop technique and an analytical method to validate computer simulation output for deformations of c-Si PV module laminates.

3. Finite Element Modelling (FEM)

The finite element modelling (FEM) and finite element analysis (FEA) are indispensable tools which have been widely used successfully to carry out research investigations. Many researchers that include [11,12,15,19-23] have effectively used the method to carry out investigations on thermo-mechanical reliability of c-Si PV module. In this research, the technique is used to validate the results obtained from analytical models. This section presents the modelling procedure adopted to carry out the investigation in three sub-sections.

3.1 The finite element (FE) model and methodology

A FE model of a standard c-Si-PV module consisting of two cells each having base area of 352000 μm by 156000 μm is created using SolidWorks software. The model is presented in Fig 1.1(b). The model consists of nine components including two interconnections. The dimensions of the constituent components are measured in micrometres (μm) and are presented in Table 1. The dimensions are close to the one used by [12,19,23]. For a sensible analytical study, a strip is cut off from the c-Si PV module shown in Fig 1.1(b) and presented in Fig 1.1(c) and Fig 3.1. The Fig 3.1 (a) is the full strip while the Fig 3.1 (b) shows the interconnection and the metallisation section of

the Fig 3.1(a). The strip presented in Fig 3.1 is used for both the analytical and simulation studies. The components and dimensions of the strip laminates are presented in Table 2.

Table 1: Dimensions of c-Si PV module component parts

Materials	Width (μm)	Length (μm)	Thickness (μm)	Number of parts
Glass	156000	352000	3600.0	1
EVA	156000	352000	450.0	2
Silicon	156000	156000	175.0	2
Aluminium	156000	156000	25.0	2
Tedlar (TPT)	156000	352000	175.0	1
Copper	3000	156000	150.0	4
SnPb Solder	3000	156000	30.0	8
Silver	3000	156000	50.0	4

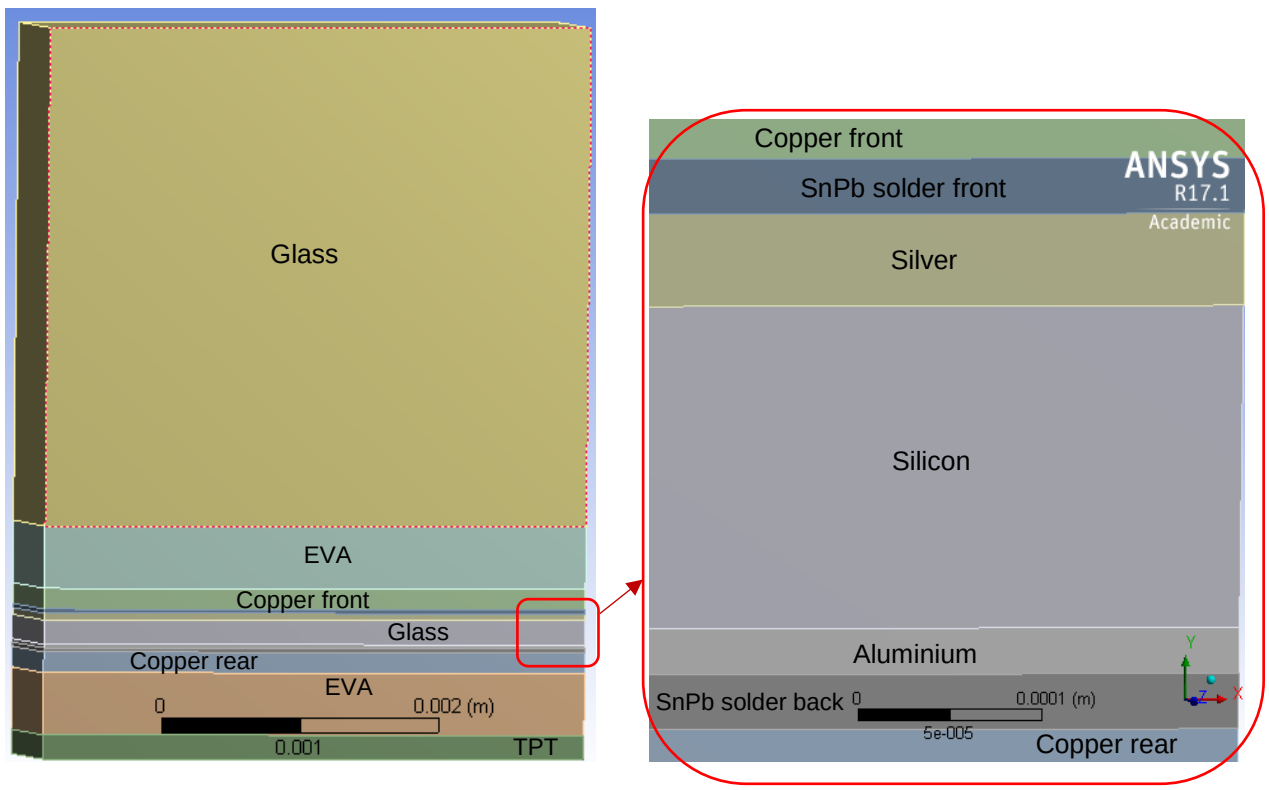

(a) (b)

Fig 3.1: A strip of c-Si PV module laminate showing:
(a) Full strip with material composition.
(b) A section of the full strip.

Table 2: c-Si PV module strip laminate components and their dimensions

Component material	Width (μm)	Length (μm)	height (μm)
Glass	1000	7000	3600
EVA	1000	7000	450
Copper (front)	1000	7000	150
SnPb Solder (front)	1000	7000	30
Silver	1000	7000	50
Silicon	1000	7000	175
Aluminium	1000	7000	25
SnPb Solder (back)	1000	7000	30
Copper (back)	1000	7000	150
EVA	1000	7000	450
Tedlar	1000	7000	175

3.2 Materials and their Properties

The materials in the c-Si PV module laminate and their mechanical properties are presented in Table 3. Solder material response to temperature load is modelled using Garofalo creep relation as well as Anand's visco-plastic model. During field operation the duration of thermal cycle of solder in the c-Si PV module interconnection is in the order of minutes to days and the solder is presumed to deform primarily due to creep. Thus creep relation has been widely used to capture the rate-dependent plasticity of solder alloys in interconnections and joints. Researchers which include [14,15,18] have successfully employed the model in similar investigations. Owing to the inability to achieve simulation of condition of low strain over a long period in a controlled laboratory because of its high demand on time and cost, the accelerated temperature cycle (ATC) or highly accelerated temperature cycle (HATC) is used as an alternative.

The flow equations of creep strain rate are:

$$\frac{d\varepsilon_{cr}}{dt} = C_1[\sinh(C_2\sigma)]^{C_3} exp^{(-Q/RT)} \quad (1)$$

$$\frac{d\varepsilon_{cr}}{dt} = C_1[\sinh(C_2\sigma)]^{C_3} exp^{(-C_4/T)} \quad (2)$$

Where $\frac{d\varepsilon_{cr}}{dt}$, *σ, Q, R and T* are the scalar creep strain rate, von Mises effective stress, activation energy, universal gas constant, absolute temperature, respectively. The other symbols represent material dependent parameters. The values of the creep parameters C_1, C_2, C_3 and C_4 are presented in Table 4.

Some schools of thought believe that solder material response to elevated temperature operation is best modelled as visco-plastic. Thus, we employ Anand's visco-plastic model separately in addition to the creep model to simulate the solder responses. The Anand's constant used to model the visco-plastic response of solder in presented in Table 5.

The visco-plastic properties of SnPb solder is extracted from Table 1 of Ye et al 2010 [14] and Table 2 of Zahn 2002 [16].

The flow equation (3) represents the Anand's constitutive model whose parameters are defined in Table 5.

$$d^p = Ae^{(-Q/RT)}\left[\sinh\left(\xi\frac{\sigma}{s}\right)\right]^{1/m} \quad (3)$$

Other parameters associated with the model and which are not defined in Table 5 such as d^p , *R, T* and σ are effective inelastic deformation rate, universal gas constant, absolute temperature and effective Cauchy stress respectively. The evolution of "*s*", is described by:

$$\dot{s} = \left\{sign\left(1-\frac{s}{s^*}\right)h_0\left|1-\frac{s}{s^*}\right|^a\right\}d^p \quad (4)$$

s^* is the saturation value of "*s"* associated with a given temperature and strain rate pair and it is described by Eq. (5) and $\hat{S}$ is a coefficient for saturation.

$$s^* = \hat{S}\left[\frac{d^p}{A}e^{(Q/RT)}\right]^n \quad (5)$$

A critical review of constitutive models for solder in electronic packaging was conducted by Chen et al 2017 [24]. They reported on the prediction capabilities, application scope, merits and shortcomings of each model. Their findings and the findings of other previous research in this area in addition to the reason presented previously informed our decision to use both the generalised Garofalo creep relation and Anand's visco-plasticity model to simulate the SnPb solder response to applied ambient temperature load.

The EVA material is modelled as temperature dependent visco-elastic material. The properties of EVA presented in Fig 2.1 are employed to extract the values of the Young's modules (E) of EVA at the temperature range of -40ºC to 85ºC at the appropriate relaxation time. Similarly, the values of the Young's modules (E) of SnPb solder at the temperature range of -40ºC to 85ºC are computed using the expression: E = 75842-152T and inputted into the Ansys' software. The T is temperature in Kelvin.

The responses of other component materials in the c-Si PV module laminates are modelled as linear elastic and isotropic materials.

Table 3: Mechanical properties of the material in the c-Si PV module [7,12,14-16,19]
(T is material property temperature in Kelvin, K)

Material	Young's modulus (GPa)	Coefficient of thermal expansion (CTE) ppm/°C	Poisson Ratio	Shear modulus (GPa)
Glass	73.1	9.0	0.17	31.24
EVA	Temperature dependent, visco-elastic (see Fig 2.1)	270.0	0.30	Temperature dependent
Copper	110	17.0	0.34	41.05
60Sn40Pb Solder	75842-152T, visco-plastic	24.5	0.35	Temperature dependent
Silver	83.0	18.9	0.37	30.29
Silicon	170	2.6	0.28	66.41
Aluminium	70.0	23.1	0.35	25.93
Tedlar	3.2	150	0.4	1.143

Table 4: Garofalo creep parameter value for SnPb solder Ye at al 2010 [14]

Parameter	C_1 (1/s)	C_2 $(MPa)^{-1}$	C_3	C_4 (K)
Value	655.67	0.074	3.3	6359

Table 5 Constants in ANAND's constitutive model for SnPb solder [19, 25]

Constant	Parameter	Value	Definition
C1	S_o (MPa)	56.33 MPa	Initial Value of Deformation Resistance
C2	Q/R (1/Kelvin)	10830	Activation Energy/ Boltzmann's Constant
C3	A (1/sec)	1.49×10^7	Pre-Exponential Factor
C4	ξ (Dimensionless)	11.0	Multiplier of Stress
C5	m(Dimensionless)	0.303	Strain Rate Sensitivity of Stress
C6	h_o (MPa)	3321.2	Hardening/Softening Constant
C7	$\hat{S}$ (MPa)	80.42MPa	Coefficient for Deformation Resistance saturation value
C8	n(Dimensionless)	0.0231	Strain rate sensitivity of saturation value
C9	a (Dimensionless)	1.34	Strain Rate Sensitivity of Hardening/Softening

3.3 Loads and Boundary conditions

The FE model of the c-Si PV module laminate shown in Fig 3.1 is subjected to 15 complete ATCs in 61 load steps. The plot of the temperature profile as a function of time is presented in Fig. 3.2. The temperature cycling testing profile is in line with the IEC 61215 established for temperature cycling testing of crystalline silicon terrestrial PV modules. The temperature range is between -40 °C and 85 °C. The temperature cycling started from 22°C, ramped up at the rate of 2 °C/min to 85°C where it dwell for 10 minutes. It was ramped down at the same rate of 2 °C/min to -40°C where it also dwell for another 10 minutes. The cycling profile was repeated for another 14 complete cycles. The FE model is simply supported to aid simplification of the structure for comparison with the analytical method. Thus, the model is assumed to be at stress free state at room temperature of 22 ^{o}C. This is the starting temperature of the thermal cycle loading. In addition, the models are assumed to be at homogeneous temperature at each load steps. Initial stresses accumulated in the interconnection from reflow soldering processes are neglected and all laminate materials are assumed to be bonded with perfect adhesion. Fig 3.3 show the FE model of the module strip laminates with adequate mesh.

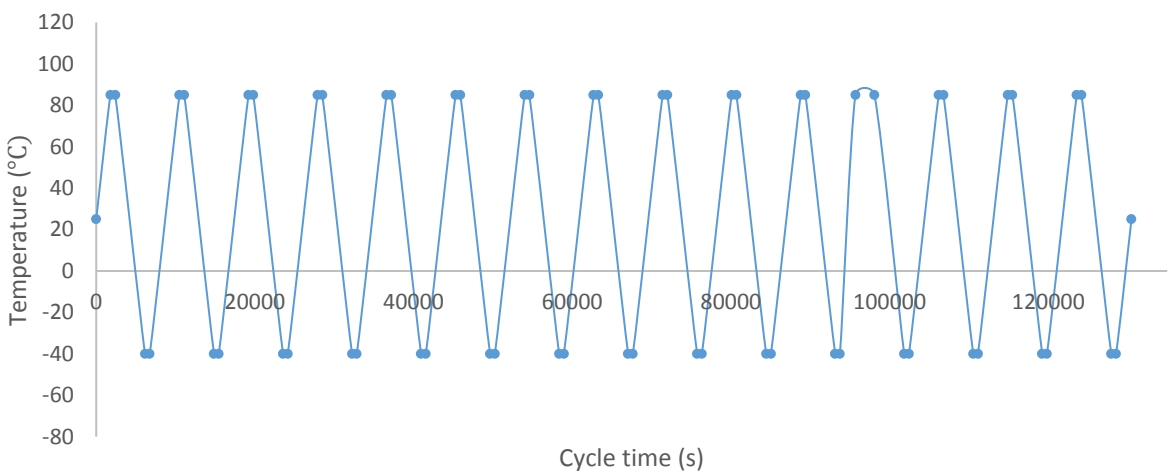

Fig 3.2: Temperature load profile as a function of time

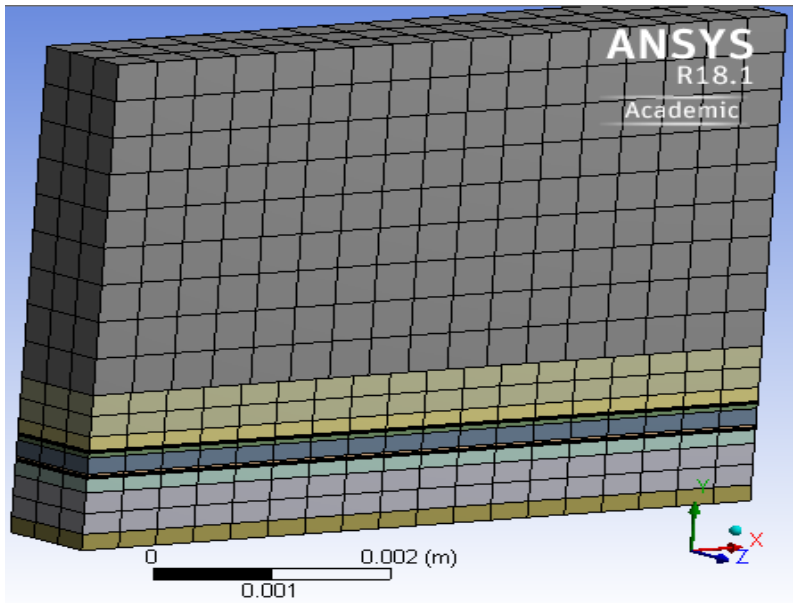

Fig. 3.3: FE model of c-Si PV module strip showing adequate mesh

4. Results and discussion

This section presents the results of the study in four sub-headings. These are: study on mechanical deformation of c-Si PV module laminates, effect of material constituents and models on c-Si PV module deformations, study on thermal expansion of c-Si PV module laminates and study on damage of solder interconnection in c-Si PV module.

4.1 Study on mechanical deformation of c-Si PV module laminates.

The degradation of c-Si PV module is measured by the deformation of the laminates in the assembly. Simplifications and assumptions based on the module geometry, materials and analysis models are critical to a successful study and development of analytical models that will predict the response of the module to induced cyclic ambient temperature. Thus, the FE model of the module is simplified to contain to a significant extent the interplay of the mechanical properties of the material bonded together in the module. The simplified model of the c-Si PV module is presented in Fig 3.1. The details of the model have been presented and discussed in section 3. For this study, the deformation is assumed to be shear-free and one dimensional. The thickness of glass is much higher than the sum of the thicknesses of the other layers. Thus, the effect of them on the expansion of glass is trivial. The assumption reduces the degree of freedom for a rational numerical analysis. Researcher paggi et al 2011 [7] reported that they treated similar model as one dimensional.

Considering Fig 3.1 and given that a virtual axial force P induces equal strain ε_i in each member of the composite. Where the ε_i may be linear elastic, visco-elastic or visco-plastic

and the i is the ith member. The axial deformation due to mechanical load P is denoted by δ_P and may be expressed thus:

$$\delta_P = \frac{PL}{EA} \tag{6}$$

$$\varepsilon = \frac{P}{EA} \tag{7}$$

$$P = \varepsilon EA \tag{8}$$

Where: $E, L\ and\ A$ are the Young's modulus, length and area of the components, respectively.

For the response of individual strip laminate considered as a beam, Eq. (8) may be written thus:

$$P = \varepsilon \sum_{i=1}^{n} E_i A_i = \varepsilon \sum_{i=1}^{n} E_i h_i w \tag{9}$$

Where: $h_i\ and\ w$ are the individual component's height and the width, respectively.

If the bonded strip is considered as one composite beam of module E^*, obtain:

$$P = \varepsilon E^* w \sum_{i=1}^{n} h_i \tag{10}$$

Combining Eq. (9) and Eq. (10), obtain:

$$E^* = \frac{\sum_{i=1}^{n} E_i h_i}{\sum_{i=1}^{n} h_i} \tag{11}$$

The response of the composite strip laminate beam to stress-strain inducement would be modelled by Eq. (12):

$$\sigma = E^* \varepsilon = \left(\frac{\sum_{i=1}^{n} E_i h_i}{\sum_{i=1}^{n} h_i} \right) \varepsilon \tag{12}$$

The Eq. (12) implicitly implies that the constitutive stress-strain relation of the composite strip laminate beam is linear elastic. Some materials of the assembly which include SnPb solder and EVA are visco-plastic and temperature dependent visco-elastic materials, respectively. Thus, Eq. (12) may not strictly model the response of the c-Si PV module to axial deformation. Considering and recognising that the two materials demonstrate low elastic modulus at the range of temperature considered, in comparison with the elastic modulus of the other materials in the laminate, the linear model is poised to represent a good fit with negligible error. This study examines this assertion and validates it in subsequent sections by employing the expression for E^* represented in Eq. (12) in numerical computation of strain energy density of solder in the c-Si PV module interconnection.

4.2 Effect of material constituents and material models on c-Si PV module deformation

To study the effect of module materials on its elastic deformation, to provide knowledge and understanding of the contribution of each material to the elastic deformation of the laminates, the concept of stiffness ratio (k_R) is employed and the laminate is considered as a composite beam. The concept measures the deformation resistance of a constituent material due to an adjacent member it is bonded to.

The stiffness of a material is denoted by *k* and expressed thus:

$$k = \frac{P}{\delta} \tag{13}$$

Where P is the force and δ is the deformation.

For an axially loaded beam, obtain:

$$k = \frac{AE}{L} \tag{14}$$

Therefore, k_R may be defined for any component, i thus:

$$k_R = \frac{k_i}{k^*} \tag{15}$$

Where: k^* denotes the stiffness of the laminate beam.

and

$$k_i = \frac{A_i E_i}{L} \tag{16}$$

and

$$k^* = \frac{A^* E^*}{L} \tag{17}$$

Thus:

$$k_{R,i} = \frac{A_i E_i}{A^* E^*} \tag{18}$$

Where: A^* denotes the area of the laminates.

Since the width of the composite strip laminate is the same for all components, Eq. (18) reduces to:

$$k_{R,i} = \frac{h_i E_i}{h^* E^*} \tag{19}$$

Where: h^* denotes the height of the laminates.

The key components of the laminates that contribute to the deformation of the module excludes the metallisation layers. Thus, the main components whose effect are studied include EVA, copper, SnPb solder, silicon and TPT. The Young's modulus of EVA at the temperature range of -40 ºC to 85 ºC temperatures is extracted from Fig 2.1. Similarly, the Young's modulus of SnPb solder is computed from the expression in Table 3.

The Eq. (19) is employed for each of the five key constituents to analytically model their contributions to the deformation of the laminates. The components EVA, copper and

SnPb solder have double layer and are treated as such. The resulting models are presented in Eq. (20) to Eq. (24):

$$k_{R,EVA} = \frac{h_{EVA}E_{EVA}}{h^{*}E^{*}} = \frac{2h_{EVA}E_{EVA}}{[2h_{EVA}E_{EVA}+2h_{Cu}E_{Cu}+2h_{SnPb}E_{SnPb}+h_{Si}E_{Si}+h_{TPT}E_{TPT}]} \quad (20)$$

$$k_{R,Cu} = \frac{h_{Cu}E_{Cu}}{h^{*}E^{*}} = \frac{h_{Cu}E_{Cu}}{[2h_{EVA}E_{EVA}+2h_{Cu}E_{Cu}+2h_{SnPb}E_{SnPb}+h_{Si}E_{Si}+h_{TPT}E_{TPT}]} \quad (21)$$

$$k_{R,SnPb} = \frac{h_{SnPb}E_{SnPb}}{h^{*}E^{*}} = \frac{2h_{SnPb}E_{SnPb}}{[2h_{EVA}E_{EVA}+2h_{Cu}E_{Cu}+2h_{SnPb}E_{SnPb}+h_{Si}E_{Si}+h_{TPT}E_{TPT}]} \quad (22)$$

$$k_{R,Si} = \frac{h_{Si}E_{Si}}{h^{*}E^{*}} = \frac{h_{Si}E_{Si}}{[2h_{EVA}E_{EVA}+2h_{Cu}E_{Cu}+2h_{SnPb}E_{SnPb}+h_{Si}E_{Si}+h_{TPT}E_{TPT}]} \quad (23)$$

$$k_{R,TPT} = \frac{h_{TPT}E_{TPT}}{h^{*}E^{*}} = \frac{h_{TPT}E_{TPT}}{[2h_{EVA}E_{EVA}+2h_{Cu}E_{Cu}+2h_{SnPb}E_{SnPb}+h_{Si}E_{Si}+h_{TPT}E_{TPT}]} \quad (24)$$

The plots of the Eq. (20) to Eq. (24) are shown in Fig 4.1. The Fig 4.1 is a plot of the normalised values of the stiffness ratios of the various components against the ambient temperature. It is observed from the figure that the degree of axial stiffness of the module laminate is hugely governed by the magnitude of the stiffness ratios of silicon solar cells and copper ribbon interconnects components. The plot shows that silicon solar cells constitute the highest stiffness ratio while the magnitude of stiffness ratio contributed by copper is 15% less than the silicon solar cells' contribution. The individual contributions of the other components are less than 10%. It may be deduced from the plot profile that the stiffness of the laminate is not hugely dependent on the ambient temperature range considered. Thus, the varying response of solder and EVA to the variations in ambient temperature does not significantly influence the stiffness of the PV module laminate. The Eq. (19) states implicitly that the higher the thickness of the component material, the more the magnitude of its stiffness ratio. The inference from the plot in Fig 4.1 and Eq. (19) is that since the silicon solar cells stiffness impact is 15% higher than copper component, their thicknesses/heights, h_i, can be used during PV module design development to design for the desired gap between solar cells. Incorrect estimation of the gap results in untimely crack initiation and subsequently module failure. The results of the FE model simulation of the stress response of the laminate to the cyclic ambient temperature is presented in Fig 4.2. The Fig 4.2 (a) shows the distribution of stress damage in the laminates while Fig 4.2 (b) shows the stress magnitudes of the critical components. The Fig. 4.2 (a) shows that the lower portion of the silicon solar cells experience greater damage and thus is more critical to failure. A closer look at the stressed components presented in Fig 4.2 [b(i) to b(vii)] reveals that the silicon solar cells with stress magnitude of 30.02 MPa is the most stressed followed by copper at the backside of the silicon solar cells with stress magnitude of 28.78 MPa. Optimal stress design to keep the silicon solar cells and interconnecting copper ribbon at the backside of the solar cells within their stress limits will increase the thermo-mechanical reliability of the c-Si PV module.

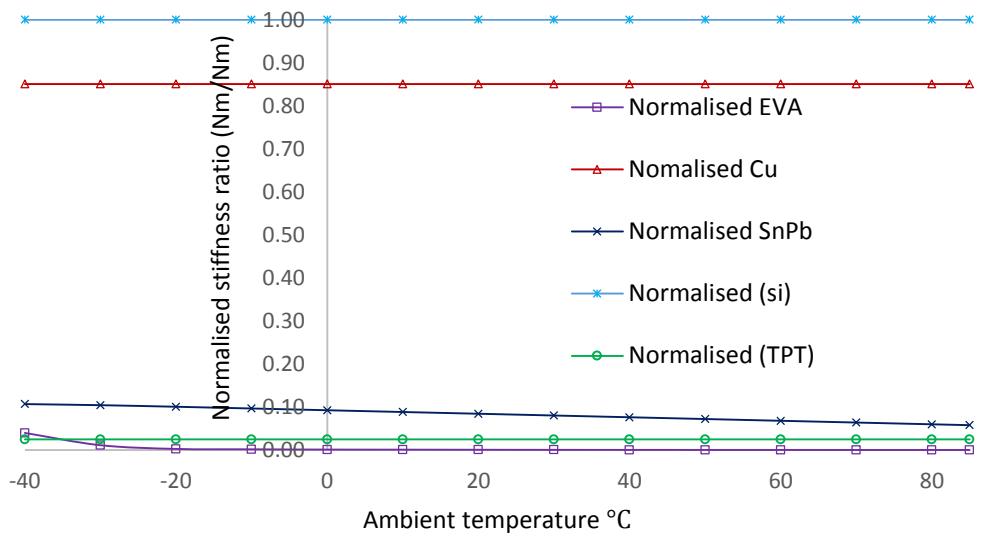

Fig 4.1: Plot of normalised stiffness ratio of the c-Si PV module materials over the thermal cycle.

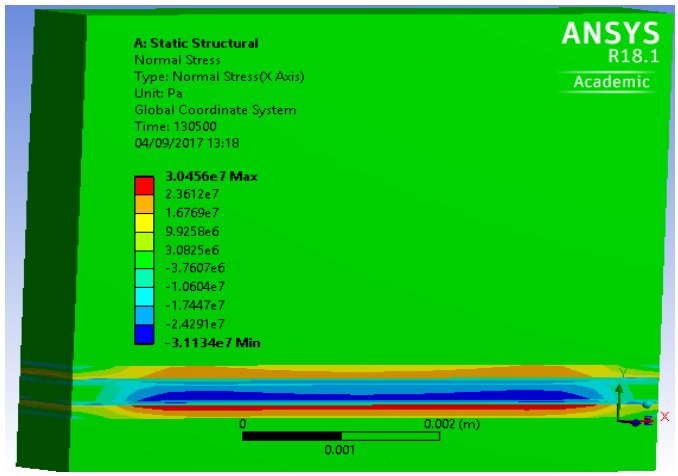

(a)

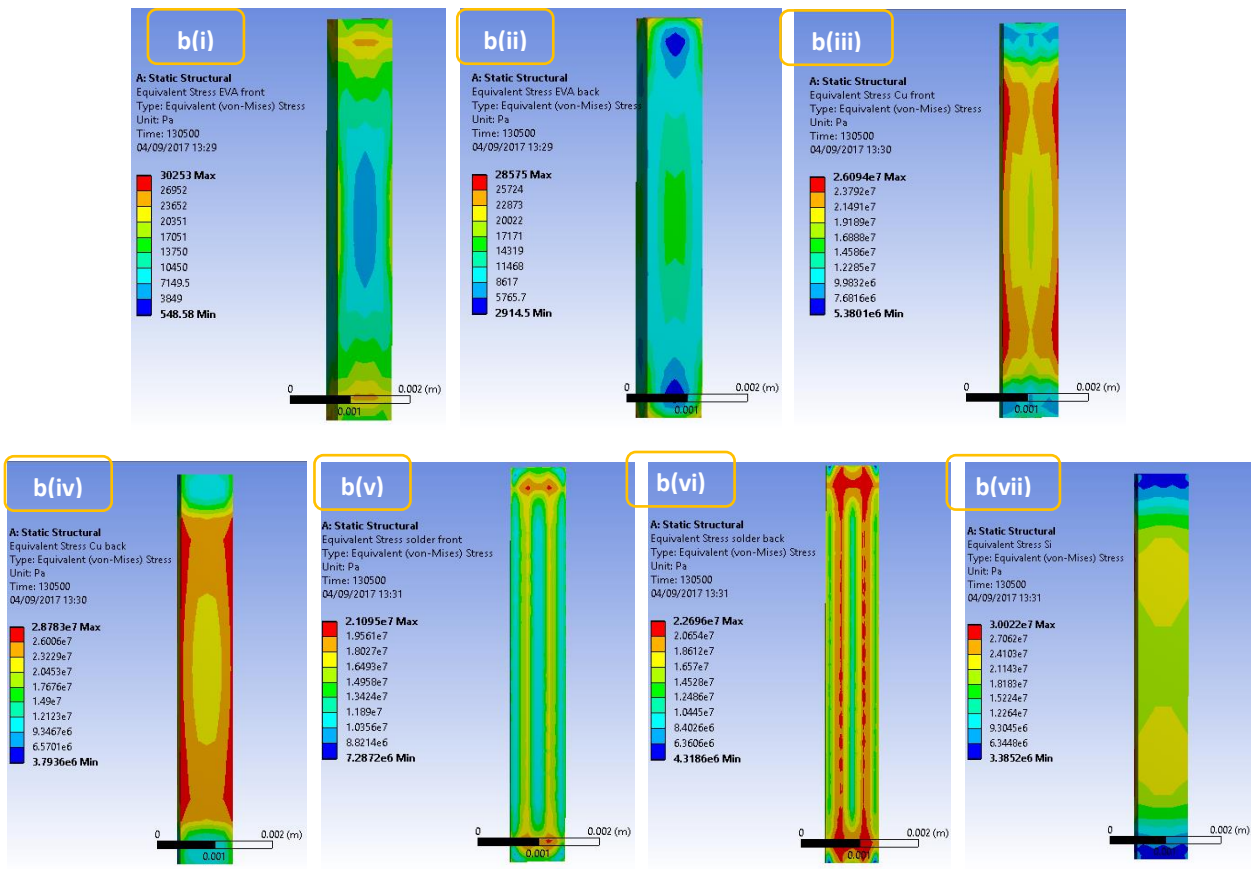

(b)

Fig 4.2: Schematic of FE model simulation of stress response of c-Si PV module laminates showing: (a) Stress concentration regions (b) Stress magnitudes of critical components.

A study of the deformation ratio of the laminates is conducted to provide a more detailed information on the contributions of the components.

Recalling the deformation Eq. (25):

$$\delta = \frac{PL}{AE} \tag{25}$$

The deformation ratio, δ_{Ri} of respective component may be expressed thus:

$$\delta_{Ri} = \frac{\delta_i}{\delta^*}$$

$$\delta_{Ri} = \frac{hE^*}{nh_iE_i} \tag{26}$$

Where n is the number of repetition of the component in the laminate. In the current study, the components EVA, solder and copper are repeated.

A plot of Eq. (26) for the various components are presented in Fig 4.3. It is a plot of the normalised deformation of the components over the ambient temperature range. The plot shows that the laminate deformation is governed by the magnitude of deformation of EVA and TPT. At 20° C temperature, EVA component constitute about 90% of the total deformation in c-Si PV module laminate while each of the components constitutes less than 10%. The TPT constitute about 0.16%. Since EVA encapsulates the solar cells, the magnitude of variations in the gap between solar cells is also governed by the degree of EVA deformation. The results of the FE model simulation of the deformation response of the laminate to the cyclic ambient temperature is presented in Fig 4.4. The Fig 4.4 (a) shows the distribution of deformation damage in the laminate strip while Fig 4.4 (b) shows the deformation magnitudes of the critical components. The Fig. 4.4 (a) shows that the middle portion of the laminates experiences greater deformation damage. A closer look at the deformed components presented in Fig 4.4 [b(i) to b(vii)] reveals that the EVA material is the most deformed component and the interface boundary between EVA and copper is critical to micro crack initiation. An optimal design intent focusing on achieving minimal solar cell gap and critical thermo-mechanical reliability may be realised by replacing EVA with material of similar properties but possessing better deformation resistance.

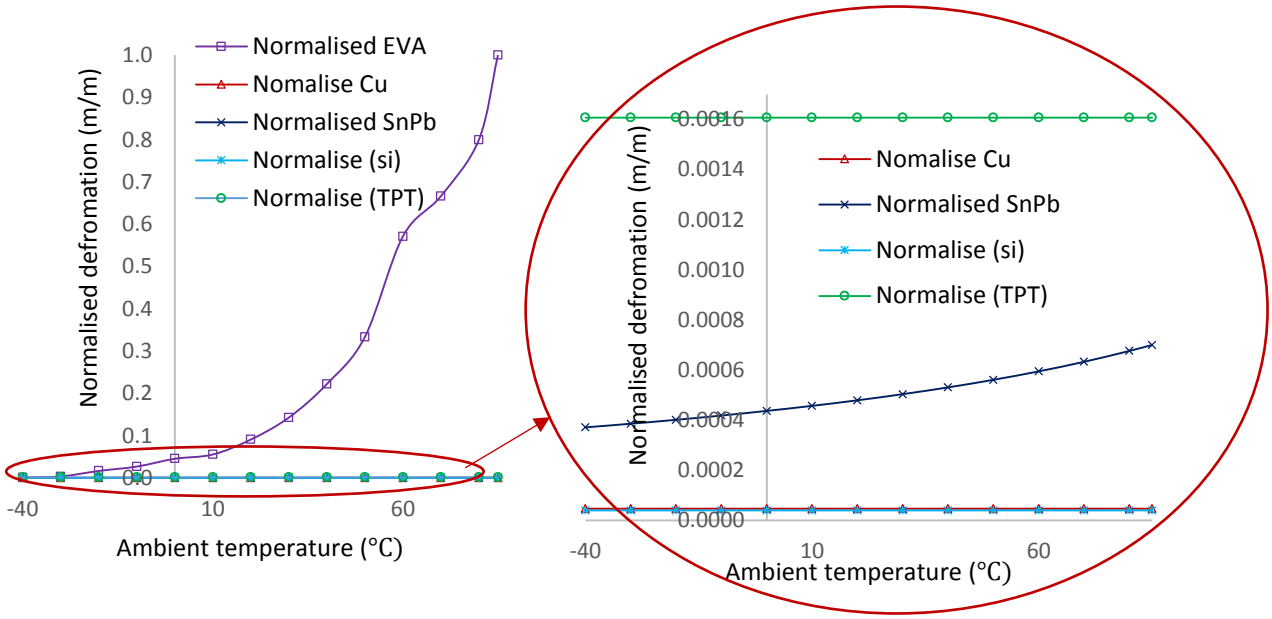

(a) (b)

Fig 4.3: Plot of normalised deformation ratio of PV module materials against ambient temperature.

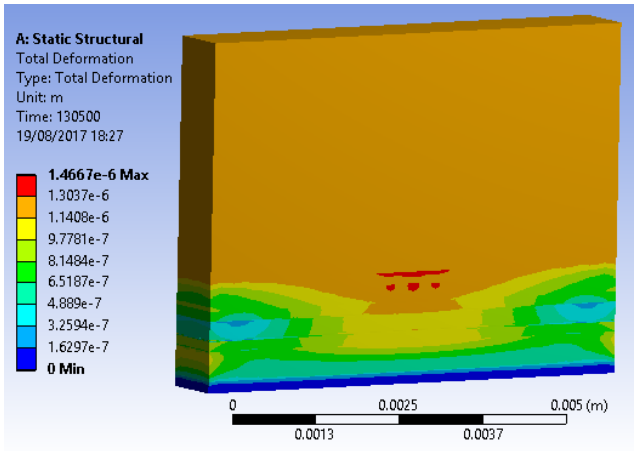

(a)

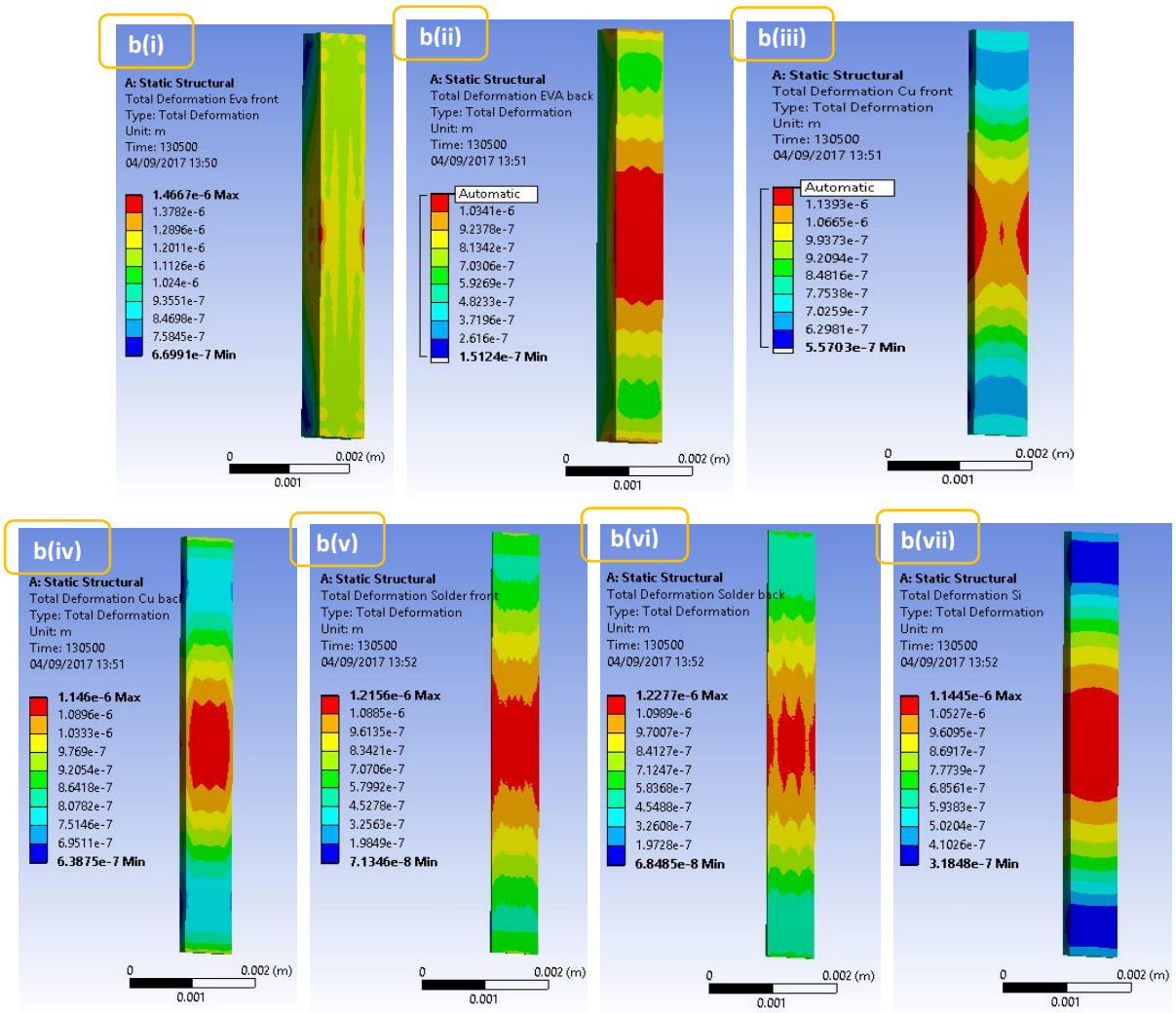

(b)

Fig 4.4: Schematic of FE model simulation of deformation response of c-Si PV module laminates showing: (b) Deformation profile (b) Deformation magnitudes of critical components.

4.3 Study on thermal expansion of the c-Si PV module

The deformation of the laminates may be considered axial thermo-elastic and temperature dependent because the laminate curvature is restricted by the constraint exerted by glass superstrate. In consideration of the observation, the axial thermo-elastic stress in the ith layer, σ_i, may be expressed as in Eq. (27) reported by Carpinteri and Paggi 2008 [26]:

$$\sigma_i = \varepsilon^* E_i - \alpha_i E_i \Delta T \tag{27}$$

Where ΔT is the change in temperature. ε^* is the strain in the laminates.

Given that the thermal deformation is caused by a virtual axial force, P, expressed thus:

$$P = \sum_{i=1}^{n} \sigma_i h_i w = 0 \tag{28}$$

Then, combining Eq. (27) and Eq. (28), obtain:

$$\varepsilon^* \sum_{i=1}^{n} E_i h_i - \sum_{i=1}^{n} \alpha_i E_i h_i \, \Delta T = 0$$

$$\varepsilon^* = \frac{\sum_{i=1}^{n} \alpha_i E_i h_i}{\sum_{i=1}^{n} E_i h_i} \Delta T \tag{29}$$

Eq. (29) may be written as:

$$\varepsilon^* = \alpha^* \Delta T \tag{30}$$

Where: $$\alpha^* = \frac{\sum_{i=1}^{n} \alpha_i E_i h_i}{\sum_{i=1}^{n} E_i h_i} \tag{31}$$

Giving that thermal expansion ratio of individual component is denoted as α_{Ri} and defined thus:

$$\alpha_{Ri} = \frac{\alpha_i}{\alpha^*} \tag{32}$$

The evaluation of Eq. (32) for the various components and a study of its plot will provide information on the material layer which governs the thermal expansion response of the laminates and thus its thermo-mechanical deformation and degradation. A plot of the normalised parameters is presented in Fig 4.5. The plot shows that the thermo-mechanical expansion of the laminate is hugely governed by the magnitude of the ratios of EVA and SnPb solder. From the plot, at 0°C temperature, the magnitude of thermal expansion ratio contributed by EVA is about 50% more than that contributed by the SnPb solder. The value widens as the ambient temperature increases. The contributions of the other materials appears to be less than 0.1%.

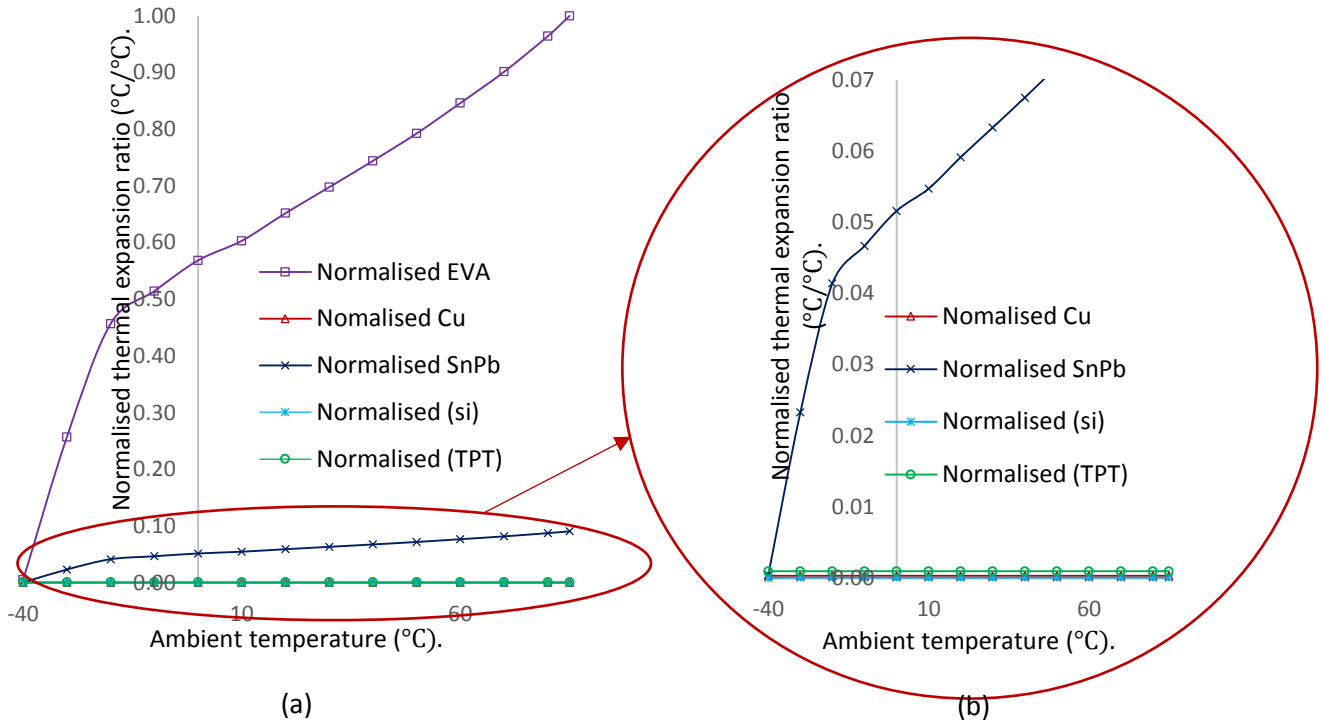

Fig 4.5: Plot of normalised thermal expansion ratio of PV module materials against ambient temperature

4.4 Study on damage of solder interconnection in c-Si PV module laminates

The five components in the laminate which include EVA, copper, SnPb solder, silicon and TPT, are used to analytically study the damage of the solder joint in the module. The magnitude of strain energy density accumulated in the solder joint is used to measure the degree of degradation and damage of the joint. The higher the magnitude, the more damaged is the joint. The applied cyclic thermal load is considered to induce fatigue load occasioned by flexural deformations in the laminates due to the mismatch of CTE of the materials bonded together in the laminates. The concept of thermal strain energy,U_T, is employed to analytically study the damage in c-Si PV module laminate under this condition in this section.

Generally, deformation in materials induces strain in the materials which they store as stain energy. The analysis of the deformation and stored energy may be done utilising the fundamental principles of Castigliano's theorem. The underlining model is presented in Eq. (33) while the applications in flexural deformations and the corresponding induced strain energy are expressed by Eq. (34):

$$\delta = \frac{\partial U}{\partial P} \tag{33}$$

$$U = \int_0^L \frac{M^2}{2EI} dx \tag{34}$$

Where: δ is deformation, U is strain energy, P is applied load, M is bending moment, E is Young's modulus and I is moment of inertia.

The flexural loading induces bending deformation that results in storage of flexural strain energy. Solder damage associated with thermal strain energy,U_T, may be expressed thus:

$$U_T = \int_0^L \frac{M^2 dx}{2EI} \quad (35)$$

Since the strip laminate is considered as a composite beam, the magnitude of its curvature ϱ may be expressed thus:

$$\varrho = \frac{1}{r} = \frac{M}{EI} = f(\delta_T) \quad (36)$$

$$\delta_T = \delta_2 - \delta_1 = L\Delta T\alpha^* \quad (37)$$

Where δ_T is the effective flexural thermal deformation of the laminates, δ_2 and δ_1 are the positive and negative deformations corresponding to concave and convex bending, respectively. The concave and convex bending arises from the thermal response of different materials bonded on top and below a reference component in the laminate. The relationship among the parameters in the interplay of net deformation arising from the difference between the positive and negative bending moment deflections in the laminates may be represented thus:

$$\frac{M^*}{E^*I^*} = \frac{1}{L\Delta T\alpha^*}$$

Where $M^*$and $I^*$are the bending moment and moment of inertia of the laminate strip.

Therefore:

$$M^* = \frac{E^*I^*}{L\Delta T\alpha^*} \quad (38)$$

Substitution of Eq (38) into Eq. (35) yields:

$$U_T = \frac{1}{2}\int_0^L \frac{E^*I^*}{L^2\Delta T^2\alpha^{*2}} dx \quad (39)$$

On integration under reasonable assumptions, Eq (39) reduces to:

$$U_T = \frac{E^*I^*}{2L\alpha^{*2}\Delta T^2} \quad (40)$$

The moment of inertia of a composite beam consisting of *n* number of components in the laminate may be computed considering Fig 4.6. For simplicity, the laminate is considered as a composite beam whose neutral axis lies at the centroidal axis on plane section xx as shown in Fig 4.6. The metallisation components are ignored as they do not constitute the key component under study. The computation of the laminate moment of inertia I^*

can be carried out by employing the fundamental moment of inertia equations to the individual components.

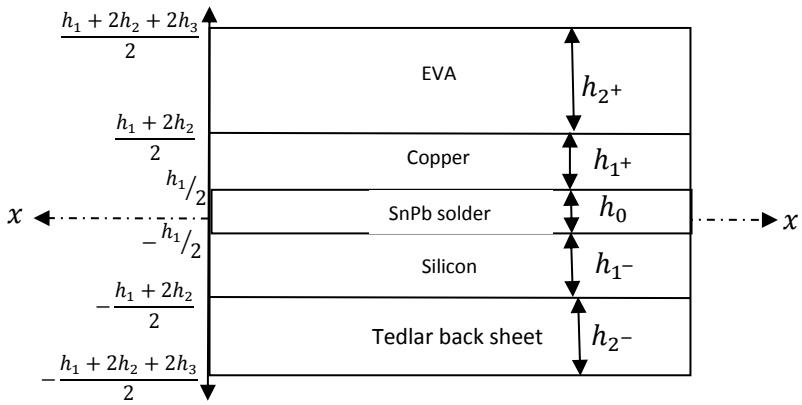

Fig 4.6: Schematic representation of the c-Si PV module laminate for I^*expression computation.

Thus, for the SnPb solder component whose centroidal axis lies at the neutral axis, obtain:

$$I_{O\,(xx)} = \int_A h^2 dA = \frac{1}{12} w {h_o}^3 \qquad (41)$$

Where $I_{O\,(xx)}$ and h_o are the moment of inertia of solder component about the centroidal axis and height of solder component, respectively.

For the other i^{th} components with a centroidal axis at a distance H_i from the neutral axis, the parallel axis theorem may be employed to obtain:

$$I_{i\,(xx)} = I_{i\,(zz)} + A_i {H_i}^2 \qquad (42)$$

Where: $I_{i\,(xx)}$ is the moment of inertia of the ith component about the neutral axis, $I_{i\,(zz)}$ is the moment of inertia about its centroidal axis, and A_i is its area.

Therefore, for the laminate, the moment of inertia I^* about the neutral axis may be computed using Eq. (43):

$$I^* = I_{0(xx)} + \sum_{i=1}^{n} I_{i(xx)} \qquad (43)$$

Thus:

$$I^* = \frac{w}{12}\left\{{h_o}^3 + \sum_{i=1}^{n} h_i \left[{h_i}^2 + 3\left(h_i + 2\sum_{j=1}^{i-1} h_j + h_0\right)^2\right]\right\}\begin{cases} i = 1: j\ does\ not\ exist. \\ i > 1: j\ exists. \end{cases} \qquad (44)$$

Where: j is the number of sandwich components between the centroidal component and the ith component, h_j is the height of the jth sandwich component.

Then: $i = 1 = \begin{cases} Copper \\ Silicon \end{cases} \quad then \quad J = 0$

And: $i = 2 = \begin{cases} EVA \\ TPT \end{cases} \quad then \quad J = \begin{cases} Copper \\ Silicon \end{cases}$

For the five components in the laminate shown in Fig 4.6, Eq. (44) becomes:

$$I^* = \frac{w}{12}\left\{{h_{SnPb}}^3 + h_{Cu}\left[{h_{Cu}}^2 + 3(h_{Cu} + h_{SnPb})^2\right] + h_{Si}\left[{h_{Si}}^2 + 3(h_{Si} + h_{SnPb})^2\right] + h_{EVA}\left[{h_{EVA}}^2 + 3(h_{EVA} + 2h_{Cu} + h_{SnPb})^2\right] + h_{TPT}\left[{h_{TPT}}^2 + 3(h_{TPT} + 2h_{Si} + h_{SnPb})^2\right]\right\} \quad (45)$$

The flexural thermal strain energy density ratio, $U_{R,i(dT)}$, for each component materials i may be denoted as $U_{R,i(dT)}$ and expressed thus:

$$U_{R,i(dT)} = \frac{E_i I_i {\alpha^*}^2}{{\alpha_i}^2 (wLh_i) E^* I^*}$$

$$U_{R,i(dT)} = \left(\frac{1}{wLh_i}\right)\left(\frac{E_i I_i}{E^* I^*}\right)\left(\frac{\alpha^*}{\alpha_i}\right)^2 \quad (46)$$

Eq. (46) implies that the $U_{R,i(dT)}$ depends on the ambient temperature implicitly and explicitly on the thickness of the components as well as the ratios of: Young's modulus, CTE and the moment of inertia of the component materials and the laminate. The Eq. (46) is implicit on temperature because the Young's modulus of EVA and SnPb solder depend on temperature. A plot of Eq. (46) for the SnPb solder component is presented in Fig 4.7.

The plot shows that solder strain energy density attains steady state values of about 43 J/m^3 over temperature range of -40 °C to 85 °C. The development of the analytical technique and model have become imperative considering the increasing application of finite element modelling (FEM) and analysis(FEA) to research investigations involving solder joints and interconnections. The method presents an alternative method to validate the results of FEM and FEA in the absence of state-of-the-art electronic laboratory. In addition, the technique presents a method of validating the results of FEA on prediction of magnitude of solder deformation damage in solder joints in both PV module interconnections and electronics assembly solder joints. Reports of varying solder strain energy damage magnitudes by numerous FEA research have been presented in section 2.

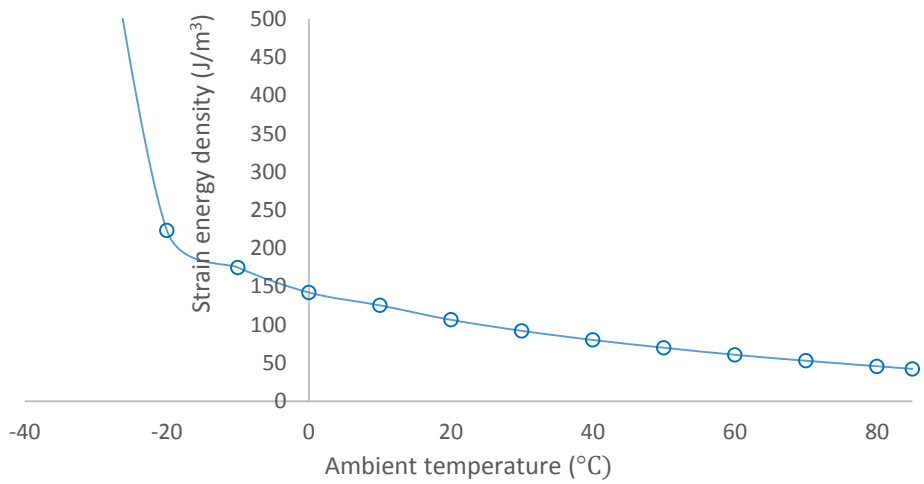

Fig 4.7: Plot of magnitude of SnPb solder strain energy density over ambient temperature.

The results of the FE model simulation of the strain response of the laminate to the induced cyclic ambient temperature are presented in Fig 4.8. The Fig 4.8 (a) shows the distribution of strain damage in the laminates while Fig 4.8 (b) shows the strain magnitudes of the solder at the front and backside of the silicon solar cells. The Fig. 4.8 (a) shows that the maximum equivalent total strain occurs at the solder on the backside of the silicon solar cells – the lower strip shown. A closer look at the strained solder components presented in Fig 4.8 [b(i) to b(ii)] reveals that the solder at the front side of the solar cells has strain magnitude of 0.0378 m/m while that at the backside has magnitude of 0.0679 m/m. This observation demonstrates that solder component is the most susceptible to strain induced failure. The observation informs the analytical study on solder strain energy damage in c-Si PV module to provide knowledge and understanding of its deformation and degradation damage mechanism for improved design.

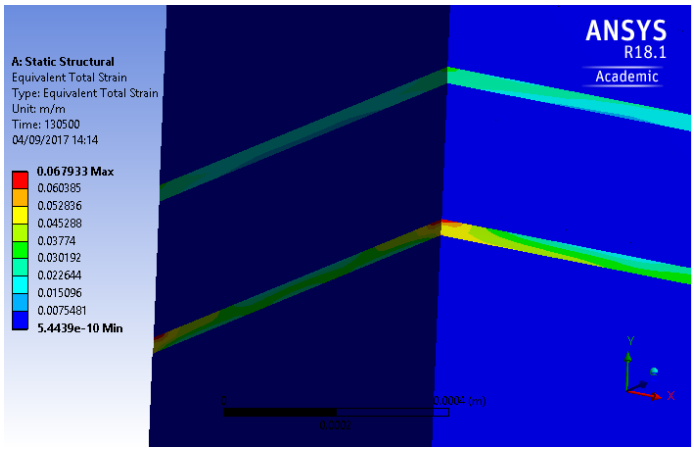

(a)

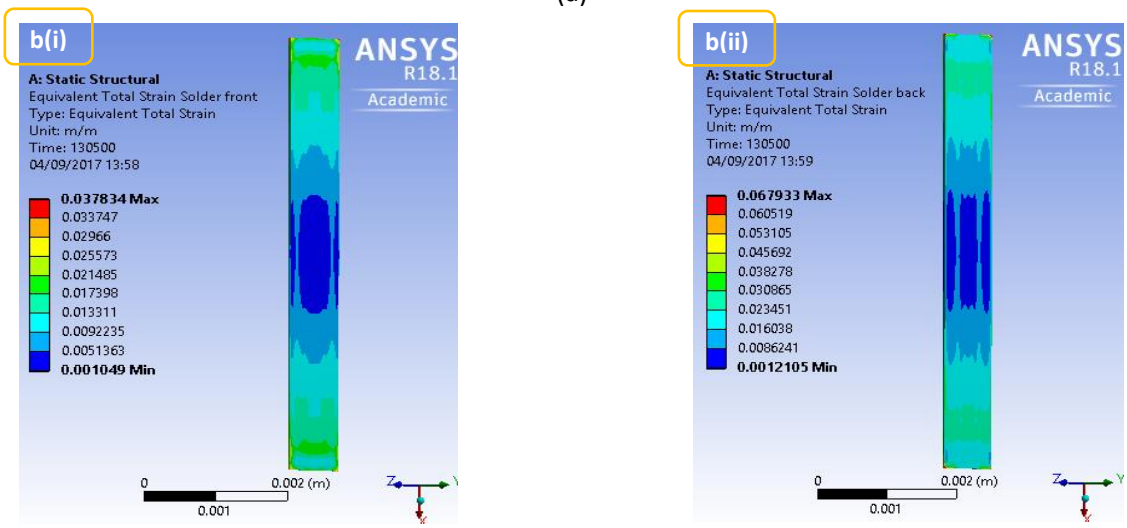

(b)

Fig 4.8: Schematic of FE model simulation of strain response of c-Si PV module laminates showing:
(a) Strain profile (b) Strain magnitudes of critical components.

Plots of the values of strain energy density of the solder obtained from simulation outputs employing the creep relation and visco-plastic model for both the solder at the front side and backside are presented in Fig 4.9. The plots demonstrate that the magnitude of steady state SnPb solder strain energy density for this assembly ranges from about 13 J/m^3 to 56 J/m^3. The range in within the 43 J/m^3 magnitude obtained from the analytical model presented in Eq. (47). The plots also show that creep values are higher than the visco-plastic values. Comparing the plots from the simulation results with the plot from the analytical model, it can be inferred that the correctness of the material models in predicting the magnitude of solder strain energy density damage depends on the geometry of the FE model. This is inferred since both the plots of visco-elastic strain

energy density per cycle (back solder) and creep strain energy density per cycle (back solder) are close to each other and also to the value obtained from analytical model.

The magnitude and nature of the distribution of the strain energy damage in the solder back and front are presented in Fig 4.10 and Fig 4.11, respectively. It can be seen that the damage in solder back is more intense.

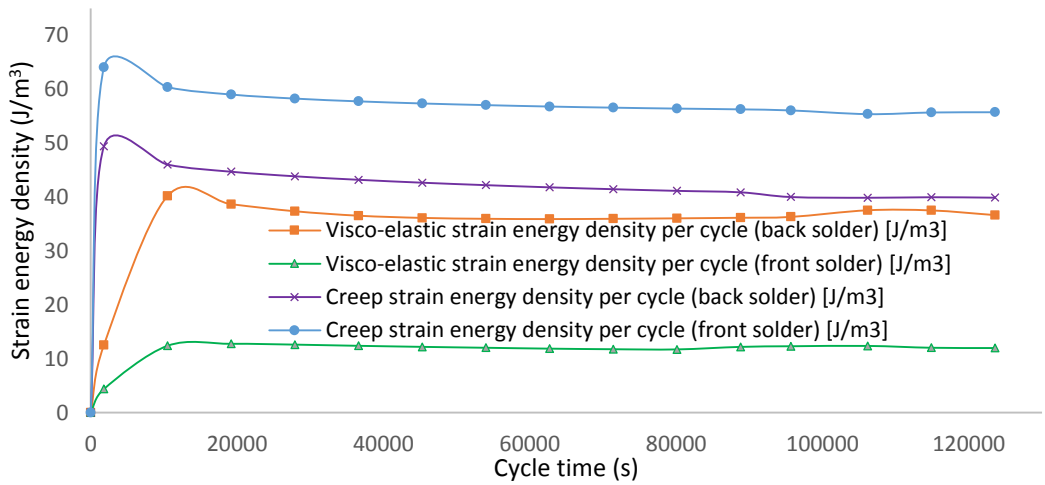

Fig 4.9: Plot of creep and visco-plastic strain energy densities from Ansys FEA simulation.

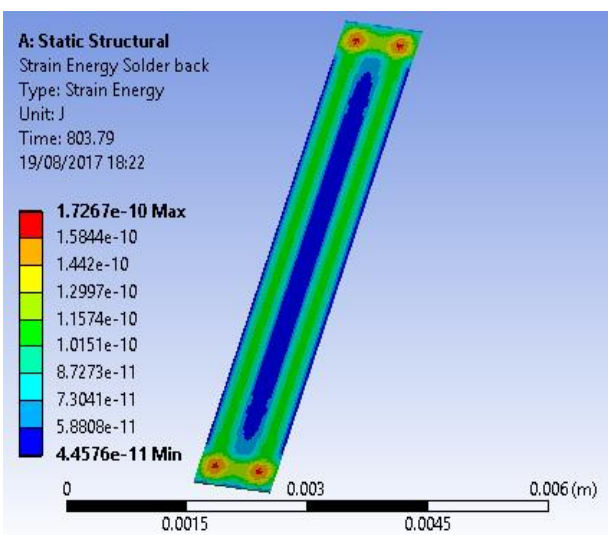

Fig 4.10: Distribution of visco-plastic strain energy on solder back showing the critical site.

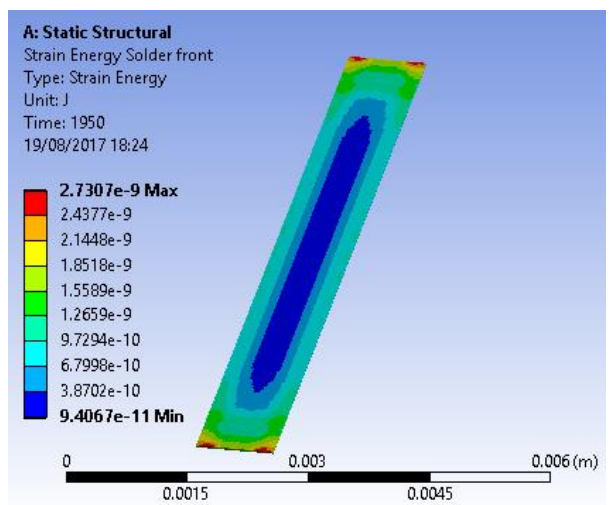

Fig 4.11: Distribution of visco-plastic strain energy on solder front showing the critical site.

5. Conclusions

Fundamental mechanics theories and principles are applied in this research to study the deformation and damage responses of materials bonded together in crystalline silicon photovoltaic (c-Si PV) module laminates. The magnitude of deformation determines the reliability of the systems and its mean-time-to-failure in addition to the failure mode. The failure is critical at elevated temperature operations. The deformation response studied include the strain energy density damage of tin-lead (SnPb) solder used to bond copper ribbons to the silver and aluminium metallization on the front and back sides of silicon solar cells. Finite element modelling (FEM) and analysis (FEA) are employed to validate the results obtained from analytical models. The study provides knowledge and techniques on how to design for deformations in c-Si PV module laminate to accommodate gaps between solar cells to avoid/minimise cell stress and cracking. The knowledge and technique will also be useful to the c-Si PV module design engineer to design for maximum fatigue life of the module up to the 25-year warranty.

The investigation has provided knowledge and technique to validate the computer simulation output results of solder strain energy density accumulated in solder joints of c-Si PV module laminates.

Based on the results obtained, it can be concluded that:

- The silicon solar cells and copper ribbon components govern the stiffness of the laminate with the solar cells being the most stressed. The solar cells stress level must be kept below yield limit.
- The ethylene vinyl acetate (EVA) is the most deformed component material and since it encapsulates the solar cells, recognising and modelling it as a visco-elastic material will improve the accuracy of design for correct solar cells gap especially for elevated temperature operations of the module.
- The SnPb solder component is the most susceptible but EVA to thermal expansion caused by ambient temperature cycling loading. Owing to solder material properties and structure in the laminates, the magnitude of accumulated solder strain energy density is critical and accelerates its degradation which makes it the most critical to fatigue induced failure. This magnitude must be kept within acceptable limit especially for elevated ambient operations to realise the 25-year module designed life and warranty.

Acknowledgements
The authors acknowledge support received from the Teesside University, UK and Staff especially Kevin Thomas, Linda Chambers and Wendy Forbes.

References

1. Ogbomo, O.O., Amalu E.H., Ekere,N.N., Olagbegi, P.O., *A review of photovoltaic module technologies for increased performance in tropical climate.* Renewable and Sustainable Energy Reviews, 2017. **75**: p. 1225-1238.
2. T., S., *Advances in crystalline silicon solar cell technology for industrial mass production. .* NPG Asia Mater, 2010. **2**(3): p. 96–102.
3. Zarmai, M.T., Ekere, N.N., Oduoza C.F. Amalu, E.H., *A review of interconnection technologies for improved crystalline silicon solar cell photovoltaic module assembly.* Applied Energy, 2015. **154**: p. 173-182.
4. McCluskey, F. *Reliability modeling for photovoltaic modules*. in *Photovoltaic module reliability workshop*. 2010. Denver, Cororado.
5. Campeau, Z., et al. (2013) *SunPower module degradation rate.* . 1–61.
6. Wohlgemuth, J., D.W. Cunningham, and A. Nguyen. *Failure modes of crystalline Si modules.* in *Photovoltaic modul Reliability Workshop.* . 2010.
7. Paggi, M., S. Kajari-Schro¨der, and U. Eitner, *Thermomechanical deformations in photovoltaic laminates.* J. Strain Analysis, 2011. **46**: p. 772-782.
8. Lyubimova, L.L., et al., *The effect of thermo-mechanical loading on fracture-related parameters of austenitic steel.* Engineering Failure Analysis, 2017. **81**(Supplement C): p. 45-56.
9. Mejri, M., et al., *Fatigue life and residual strength of a short- natural-fiber-reinforced plastic vs Nylon.* Composites Part B: Engineering, 2017. **110**(Supplement C): p. 429-441.
10. Khashaba, U.A., A.A. Aljinaidi, and M.A. Hamed, *Fatigue and reliability analysis of nano-modified scarf adhesive joints in carbon fiber composites.* Composites Part B: Engineering, 2017. **120**(Supplement C): p. 103-117.
11. Pandder, M., et al., *Thermo-mechanical assessment of solar cell displacement with respect to the viscocoelastic behaviour of the encapsulant*. 2011.: Int. Conf. on thermal, mechanical and multiphysics simulation and experiments in microelectronics and microsystems, EuroSimE. p. 1-6.
12. Bosco, N., T.J. Silverman, and S. Kurtz, *Climate specific thermomechanical fatigue of flat plate photovoltaic module solder joints.* Microelectronics Reliability, 2016. **62**: p. 124–129.
13. Eitner, U., et al. *THERMOMECHANICS OF PV MODULES INCLUDING THE VISCOELASTICITY OF EVA*. in *26th European Photovoltaic Solar Energy Conference and Exhibition*.
14. Ye, H., et al., *Reliability evaluation of CSP soldered joints based on FEM and Taguchi method.* Computational Materials Science, 2010. **48**(3): p. 509-512.
15. Park, N., J. Jeong, and C. Han, *Estimation of the degradation rate of multi-crystalline silicon photovoltaic module under thermal cycling stress.* Microelectronics Reliability, 2014. **54**(8): p. 1562-1566.
16. Zahn, B.A. *Impact of Ball via Configurations on Solder Joint Reliability*. in *Electronic Components and Technology Conference* 2002. San Diego, CA.
17. Zahn, B.A. *Solder Joint Fatigue Life Model Methodology for 63Sn37Pb and 95.5Sn4Ag0.5Cu Materials*. in *Electronic Components and Technology Conference*. 2003. New Orleans.
18. Cuddalorepatta, G., et al., *Durability of Pb-free solder between copper interconnect and silicon in photovoltaic cells.* Progress in photovoltaics: Research and applications., 2010. **18**: p. 168-182.
19. Bosco, N., T.J. Silverman, and S. Kurtz, *The Influence of PV Module Materials and Design on Solder Joint Thermal Fatigue Durability.* IEEE JOURNAL OF PHOTOVOLTAICS, 2016. **6**: p. 1407-1412.

20. Hasan, O., A.F.M. Arif, and M.U. Siddiqui. *FINITE ELEMENT MODELING AND ANALYSIS OF PHOTOVOLTAIC MODULES*. in *ASME International Mechanical Engineering Congress and Exposition*. 2012. Houston, Texas, USA.
21. Meyer, E.L. and E.E. Van Dyk, *Assessing the reliability and degradation of photovoltaic module performance parameters.* IEEE Transactions on Reliability, 2004. **53**(1): p. 83-92.
22. Paggi, M., M. Corrado, and I. Berardone, *A global/local approach for the prediction of the electric response of cracked solar cells in photovoltaic modules under the action of mechanical loads.* Engineering Fracture Mechanics 2016. **168**.
23. Paggi, M., M. Corrado, and M.A. Rodriguez, *A multi-physics and multi-scale numerical approach to microcracking and power-loss in photovoltaic modules.* Composite Structures, 2013. **95**: p. 630–638.
24. Chen, G., X. Zhao, and H. Wu, *A critical review of constitutive models for solders in electronic packaging.* Advances in Mechanical Engineering, 2017. **9**(8): p. 1–21.
25. Wang, G.Z., et al., *Applying Anand Model to Represent the Viscoplastic Deformation Behavior of Solder Alloys.* J. Electron. Packag 1998 **123**(3): p. 247-253
26. Carpinteri, A. and M. PAggi, *Thermo-elastic mismatch in nonhomogenous beams.* Journal of Engineering Mathematics., 2008. **61**: p. 371-384.